Ryan Dale

Title:
Using diffusion MRI technique as a tool in the early detection of Alzheimer's Disease

Student: Ryan Dale

Supervisor: Dr. Benedict Albensi

Department: Pharmacology

Summary:
Alzheimer's Disease (AD) is a neurodegenerative disorder that currently affects an estimated 500 000 Canadians, a prevalence that is expected to double within the next 25 years. It is projected that AD will impact the lives of one in every three Canadians over the age of 80. This disease is responsible for billions of dollars of healthcare spending every year and represents a massive burden for the patient, their family and the healthcare professionals involved in their care.
Currently, the diagnosis of any progressive dementia as Alzheimer's Disease has been based on clinical findings; a designation that can only be confirmed via post-mortem autopsy, where the presence of accumulated beta-amyloid plaques, neurofibrillary tangles and astrocytic gliosis can be confirmed. These microstructural changes have been so far undetectable in the early stages of the disease, before the clinical aspects of the dementia are manifested and a method that would allow the early detection of these changes could represent an invaluable tool.
Diffusion tensor imaging (DTI) is a type of MRI imaging that focuses on the movement of water through tissues. DTI has shown great versatility as a diagnostic tool and may be useful in the differential diagnosis of AD. This research project is aimed at exploring the utility of using DTI to detect the changes associated with Alzheimer's Disease using a transgenic animal model of AD. With earlier detection, the opportunities for drug discovery and other therapeutic interventions become possible.

Acknowledgements:
This research would not have been possible without the support entirely (or in part by);

-CIHR
-Dr. H.T. Thorlakson Foundation
-Dr. Peter Nickerson, Associate Dean (Research)
-St. Boniface Research Foundation
-MMSF
-MHRC
-Faculty of Medicine
-Health Sciences Centre Research Foundation

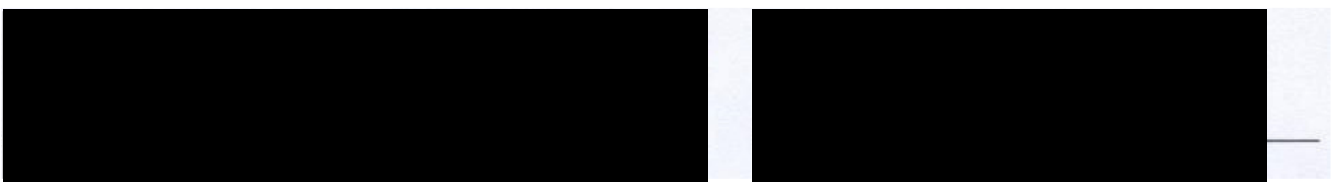

Ryan Dale

Introduction:
Alzheimer's disease (AD) is a neurodegenerative condition of memory impairment. It represents the most significant cause of disability in all Canadians over the age of 65 and currently affects the lives of over 500 000 individuals. The condition manifests itself as a progressive cognitive decline that develops into dementia typically before any other sensory or motor disturbances, meaning that for many individuals the impairment is gradual and, once present, irreversible. Patients usually die within 7-10 years of the initial diagnosis of AD, most commonly due to pneumonia complicated by decreased patient mobility and muscle wasting. The lives of patients, families, communities and professional care-givers are all greatly impacted by AD for its immense burden on financial and emotional resources, represented by billions of dollars spent and hours of care provided every year. As our population ages, the prevalence of AD in Canada is only expected to rise(1).

Alzheimer's Disease represents the most common form of neurodegenerative dementias. It is characterized by the presence and deposition of amyloid-β plaques onto the extracellular surface of cortical neurons and an associated intracellular accumulation of neurofibrillary tangles. The build-up of these two hallmark neurohistological changes also results in a generalized reactive astrocytic gliosis(2). The precise pathogenesis of AD remains unclear; it is hypothesized that the primary cause of AD is excess amyloid-β deposition which induces the neurofibrillary tangle formation. Amyloid-β, a peptide of variable length (38-43 amino acids) has two forms significant to AD; a soluble form (Aβ40) that has shown to have synaptotoxic effects during the very early stages of amyloid overproduction, and an insoluble form (Aβ42) that collects into the amyloid plaques(3). While the exact mechanisms that lead to plaque formation remain unclear, it is generally accepted that disruption of the amyloid pathway is clearly implicated in AD pathology.

There are two main types of Alzheimer's Disease. The first type, so-called “sporadic” or “late-onset” AD, appears in the seventh decade of life and represents the vast majority of cases. These can arise from a variety of reasons and risk factors and have recently been associated with the apolipoprotein ε4 allele (apo ε4), which is involved in the degradation of Aβ proteins. A second type, so-called “familial” or “early-onset” AD, arises around age 50 in between 5-7% of cases. These cases typically are found, as the name suggests, through familial lineages and have been asssociated with mutations to the amyloid precursor protein or the presenilins resulting in Aβ overproduction. Other environmental factors have been implicated in the development of AD such as traumatic brain injury, stroke, hypertension, atherosclerosis, diabetes, or any other factor that could disrupt the blood-brain barrier (some debate now revolves over whether the primary inciting factor leading to AD is actually due to BBB disruption)(4). While the research is encouraging, there remains no screening test, genetic or otherwise, that can determine a persons likelihood for developing AD, or even if the preclinical stages of AD have already begun. For decades, the only way to reliably assess the presence of any actual neurohistological changes are by taking a sample; either via biopsy or at autopsy.

The earliest affected regions of the brain appear in the hippocampus and entorhinal cortex, spreading to the association areas in the prefrontal lobe and temporoparietal junction(5). This results in the impairment of declarative memory consolidation. To the individual, these preliminary changes may be a mild or imperceptible cognitive impairment and is exceptionally difficult to detect by physicians. As the neurotoxic effects of the amyloid deposition progress, widespread cortical atrophy develops leading

ultimately into dementia, which typically precedes the clinical diagnosis of AD(6). By this point, the insidious nature of the progression and the damage done by the toxic effects of the amyloid deposition is irreversible. Recently, the development of CSF assays that can gauge the levels of CSF-Aβ and amyloid depositions, as well as positron emission tomography (PET) scans using radio-labelled glucose have provided some ability to stage the progression of the disease once it is present, but by this point the changes are well established(7). As there remains no non-invasive way of diagnosing the early development of sporadic AD, treatment strategies have historically been implemented once the clinical diagnosis has been made with a focus on slowing disease progression(8).

Magnetic resonance imaging (MRI) has established itself as an invaluable tool of the medical profession over the last 30 years. It acts as a complex type of spectrometer; MRI utilizes the inherent electromagnetic properties of certain atomic nuclei to react when struck by a radio-frequency specific to that isotope, referred to as the Larmor frequency (ω). The Larmor frequency is a product of two factors, the gyromagnetic ratio (γ essentially a constant) and (B), the magnitude of the magnetic field in which it is being applied(9):

$$\omega = \gamma B$$

When an object is placed in a strong magnetic field, the atomic nuclei that comprise that object will begin to orient their spin (the magnetic moment) to match the field. When a signal that matches the larmor frequency is applied to the sample, the nuclei that respond to that frequency will “resonate” and emit an RF signal (the free induction decay, or FID) that can be detected by the MRI equipment. By using a complex mathematical process called a fourier transformation, the detected signal can be converted from a function of time back into a function of frequency. This allows the individual signals to be reconstructed back into a theoretical 2-D space called the k-space that can produce an image based on the intensity of each individual frequency. By repeating the signal acquisition over, multiple k-spaces can be acquired. This allows a 3-D image to be developed from a 2-D series of slices. By modifying the timing of the signals, the MRI can be weighted to produce a higher intensity signal from fat (T1 weighting) or water (T2 weighting) , whichever is more relevant to the scanner(9).

Diffusion-weighted imaging (DWI) is a modified form of T2-weighted MRI that specifically focuses on the RF signal that water produces(10). It works because living tissues are anisotropic; that is, the ability for water molecules to diffuse through tissues in different directions is dependent on the tissues themselves. Two radio-frequency signal pulses of a specific value (the b-value) are applied for a given direction to a subject for a known duration and spaced apart by a known interval; the first signal induces movement of the water molecule and the second signal attempts to do the same by repeating the b-value for that particular direction. In tissues where diffusion is permitted (such as grey matter), the recorded “response” to the second signal will be decreased because the water molecules were allowed an opportunity to move around from their starting point. By calculating the difference between the signals acquired after applying each b-value (and controlling for other variables) using the Stejskal-Tanner equation, the diffusivity of a tissue can be calculated:

$$S/S_0 = e^{[-\gamma 2G2\delta 2(\Delta-\delta/3)D]}$$

Where S_0 is the signal intensity before diffusion weighting(after A0 is applied), S is the intensity after B0 is applied, γ is the gyromagnetic ratio, G is the strength of the diffusion gradient pulse applied, δ is the duration of the applied pulse, Δ is the time between the pulses and D is the Diffusion coefficient for that tissue. The diffusion coefficient data can then be reconstructed in a way similar to traditional MRI into a k-space that produces a 2-D representation of the diffusion(11).

Diffusion tensor imaging (DTI) takes diffusion-weighted imaging several steps further by scanning the target from multiple directions, using variable RF pulse gradients. By acquiring at least six different diffusion-weighted images of the same pixel along multiple orientations, the diffusion data can be (through a complex mathematical process called diagonalization) converted into six values: three eigenvalues ($\lambda 1$, $\lambda 2$ $\lambda 3$) and three eigenvectors (V1, V2, V3). These six values represent the directionality of the diffusion and can be used to reconstruct a three-dimensional shape known as a voxel. The orientation of these oblong spheroid shapes can be used to make inferences of the path that water is able to make through a tissue(11). This becomes especially relevant when considering that water diffusion along most directions is normally extremely restricted in axons. This allows DTI studies to reconstruct the patterns of white matter tracts in the brain and also to locate microstructural differences in tissues that would suggest damage or insidious pathology was present(12).

One of the challenges associated with DTI scanning is the high susceptibility to motion that the scans themselves have(13). The tracking of water molecules during signal acquisition requires that very little motion occurs between images; in humans, this requirement for stillness can be explicitly explained before the scan. Mice, however, require anaesthetic and head mounts to stay still, so the speed of the acquisition becomes a factor in successfully acquiring the data(14). One method devised to expedite the scans is called echo-planar imaging, or EPI. In contrast to normal MRI scans which typically acquire an image in a “line by line” fashion by sending a series of radio-frequency pulses (figure 1), EPI reconstructs the entire image with one prolonged RF pulse. The pulse quickly scans every line of the slice, producing an image in a much shorter period of time (figure 2). This benefit is two-fold; firstly it allows the scans to be completed much more quickly, and secondly, the scans can be repeated and averaged into one output image, which reduces the variability of the individual scans and improves the precision of the acquired data(15).

Recently, studies have suggested that DTI could provide a reliable and non-invasive means to examine the brain for changes associated with AD pathology. Pilot studies using small patient populations of individuals diagnosed with varying stages of MCI and AD have used DTI to detect changes in the areas most associated with the early development of AD, namely the hippocampus and entorhinal cortex. Elevations in the mean diffusivity (MD, also known as the apparent diffusion coefficient or ADC) were particularly seen in the hippocampus of patients with MCI and fractional anisotropy (FA) was also elevated, albeit to a lesser degree(16). Mean diffusivity is the average of all three acquired eigenvalues:

$$\mathbf{MD = (\lambda_1 + \lambda_2 + \lambda_3)/3}$$

while fractional anisotropy is a scalar description of the diffusivity of water through a tissue:

Ryan Dale

$$FA = \frac{\sqrt{3}}{\sqrt{2}} \frac{\sqrt{(\lambda_1 - \lambda)^2 + (\lambda_2 - \lambda)^2 + (\lambda_3 - \lambda)^2}}{\sqrt{\lambda_1^2 + \lambda_2^2 + \lambda_3^2}}$$

This change in the MD and FA values in the hippocampus and entorhinal cortex in possible and probable AD have been the subject of increased study over the past few years, using human subjects identified clinically as having MCI or AD using verbal and cognitive-based testing(16). This project will aim to examine whether these changes in grey matter composition can also be observed in an AD model.

The goal of this project has been to explore the potential utility of using DTI methods to detect the changes associated with Alzheimer's within an animal model, the 3xTg triple transgenic mouse. This animal model was developed by Oddo and colleagues in 2002 to express three phenotypes associated with AD pathology; the human amyloid precursor protein (Swedish mutant) transgene, the presenilin knock-in mutation, and the tau P301L mutant transgene(17). The animals are considered to have established AD pathology present by approximately 12 months of age. This has provided a useful model for drug discovery and allows researchers an opportunity to correlate data from DTI studies to the histopathological sections post-mortem (a step that has proven challenging when working with human subjects). If DTI can permit researchers some insight into the changes associated with these pathologies, especially at a stage before the clinical dementia has manifested, an opportunity for earlier interventions and novel drug discovery of this debilitating condition presents itself.

Materials and Methods:

Eight 3xTg mice were bred and aged to 12-14 months, along with eight age-matched C57 controls, according to protocols established by the St. Boniface and University of Manitoba animal care centres. Inhaled isofluorane (5.0% for induction, 2.0-2.5% for maintenance during scans) in a mixture of 30:70 O_2:N_2O was used as the anaesthetic during the procedure and the animals were maintained in position using a nose cone with attached bite bar. Respiration rate was monitored and maintained between 40-100 breaths/minute by using an electronic gating system (SA Instruments model 1025L small animal gating system) and body surface temperature of the animals was maintained throughout the procedure between 37.0-38.0^{O}C via a fluid-filled heating pad connected to a water bath. Total time under anaesthetic during preparation and scanning for each animal was approximately 75 minutes.

Animals were scanned in a Bruker Avance III horizontal bore small-animal MRI at 7.0T using Paravision 5.0 software. A 30mm quadrature birdcage coil was utilized to increase signal intensity from the head during the scans. After global shimming and signal mapping procedures, half-fourier single-shot turbo spin echo scans (HASTE) were used to ensure correct orientation within the magnet bore(18). Once corrected for orientation, a rapid-acquisition with relaxation enhancement T2 scan (RARE) was performed to produce reference images for each of three slices, using the anterior horn of the corpus callosum as a visible landmark for placement of the first slice (TR=1640ms, TE=80.0ms, FA=180^{O}, 1.00mm thick/2.00mm apart, FOV 3.0cm, in a 256x256 matrix) Acquisition time for this scan was 10m29s760ms(figure 3)(19). DTI-EPI scans were then performed using a six-directional approach for each of three slices (3 A0 scans, six B0 scans with max. B-value=1553.56, TR=1250ms, TE=26.6ms, FA=90^{O}, 1.00mm thick/2.00mm apart, FOV=3.0cm, in a 128x96 matrix autofilled to

128x128). The scan was acquired in 4 segments and the results were compiled from an average of 32 sequentially repeated scans. Total acquisition time for the DTI-EPI scan was 24m00s01ms(20). For both the RARE and DTI-EPI scans, a series of five fat-signal suppression slices were utilized in a pentagon shape around the brain slice to reduce the signal of non-target tissues by saturating the area with a signal 1230ms prior to the DTI-EPI signal(15). This resulted in the signal from these saturated areas being "off-sync" with the unaffected tissue during signal recieving and as a result, the signal from these areas during the actual acquisition was especially weakened to prevent any corruption of the target regions.

Reconstruction of scan data was accomplished using native Bruker software. The first slice scanned was used only for positioning of the second and third slices, which contained the target regions of the study. Regions of interest were defined on a slice-by-slice basis using a stereotactic mouse atlas and traced by hand. The right and left hippocampus at -2.20mm to bregma (figure 4a)and right and left median entorhinal cortex at -4.20mm to bregma (figure 4b) were traced and the signal from each area examined using signal-to-noise ratio calculators in the Bruker software. The second and third slices were also examined for signal changes as the left and right hemispheres, as well as overall changes to the whole slice itself. Mean and standard deviation values for each region of interest were used to perform two-tailed t-tests in order to compare the means of both sample populations. No results were excluded from the compiled data analysis, providing an n=8 for each sample region.

All 16 mice were euthanized at the end of the study via humane cardiac perfusion of formalin, as per accepted Canadian Council for Animal Care protocols(21). The cadavers were then decapitated and the brains dissected, collecting the hippocampus of all subjects for histological sectioning to correlate with the DTI scan results. Slices of 6μm thickness will be prepared and treated with Congo Red (for beta-amyloid localization) as well as immunohistofluorescence studies of other proteins of interest. The results of the histological sections will then be compared to the results of the DTI scanning at a future date.

Results:

Representative examples of the acquired scans and examples of the regions of interest focused on for the study are listed as Figures 3 through 6. Values of the fractional anisotropy calculated for the mean of the 3xTg mice (n=8) and the C57 controls (n=8) are displayed in Table 1. Values for the mean diffusivity calculated for the mean of the 3xTg mice (n=8) and the C57 controls (n=8) are displayed in Table 2. There were no significant differences found between the DTI data of any of the groups ($p>0.05$). The histological analysis of the 16 mice was not completed as of this writing and as a result there is no comparison between the DTI data and the physical microstructure of the subjects. This will be completed at a later date by lab representatives.

Discussion:

The study was unable to find a significant statistical difference between the FA and MD values in the 3xTg mice when compared to their C57 controls. This study may have benefited from an increased sample size that would have allowed for the increased likelihood of a Gaussian distribution of data. Due to the small size of the study (n=8 for all groups), no animals were excluded and it is entirely

possible that the influence of a larger group on the data might show a more significant result. There was a great amount of variability in the fractional anisotropy (FA) data and the acquired scans had a large degree of error in them (Table 1). This is partly due to the motion of the animals during scanning and also partly because the scans utilized only six diffusion directions, as opposed to thirty or more. Studies have shown that FA is much more variable in grey matter when compared to white matter and it was not expected that the FA would produce a significant result when focusing on the grey matter targets selected for the study(22). When white matter tracts are being scanned, a benefit to the quality of the FA has been shown in increasing the number of gradient directions when constructing the tensor(13). The mean diffusivity (MD), a localized average of the diffusivity that is accomplished sufficiently using only six diffusion directions, has been shown to be one of the earliest detectable changes in the FA and MD (which was the opposite result of what was predicted) but still no significant difference between the 3xTg and C57 groups (Table 2). This could be for a myriad of reasons, including the size of the study, the motion during the scanning, the inability for more robust post-processing and the inexperience of the experimenter. Diffusion tensor imaging represents a technique in MRI that has been around for barely twenty years; while the advancements have been immense, there is still much to learn in order to fully utilize the potential of the technique. As research using this method continues, our ability to use DTI as a diagnostic tool will only expand.

Diffusion tensor imaging was initially posited in 1990 and is based on several previously understood mathematical concepts: the tensor and the Stejskal-Tanner equation. The concept of a tensor was originally discussed by Carl Friedrich Gauss in the nineteenth century (although it was not referred to as such)(24). The development of modern tensor analysis is credited to Gregorio Ricci-Curbastro and his student, Lugo di Romagna, as a part of their landmark paper from 1900, “Methods for Absolute Differential Calculus and their applications”(25). Tensor calculation is a process that combines six vectors into a three-dimensional representation of an ellipsoid. A six-directional diffusion tensor matrix looks like:

$$\underline{\underline{D}} = \begin{pmatrix} D_{xx} & D_{xy} & D_{xz} \\ D_{yx} & D_{yy} & D_{yz} \\ D_{zx} & D_{zy} & D_{zz} \end{pmatrix}$$

Tensors have proven useful in many fields of physics and engineering and have been used previously to combine electromagnetic signal vectors in order to describe electromagnetic fields. The Stejskal-Tanner equation was first devised using NMR in 1965 based on observations that the decrease of a pulse gradient signal could be related to the diffusion of water through anisotropic mixtures. This equation is actually based on an earlier one, the Bloch-Torrey equation, that describes the change in the magnetization of a nucleus within an electromagnetic field that is due to diffusion through an isotropic substance(26):

$$M_+(\vec{r},t) = M_0 e^{-\frac{1}{3}D\gamma^2 G^2 t^3} e^{-j\gamma\vec{r}\cdot\int_0^t dt'\vec{G}(t')}.$$

A physician (and physicist), Denis le Bihan, devised the first clinical application for the Stejskal-Tanner equation by developing a technique to display the acquired diffusion data after mapping it correctly to the acquisition tissues(17). While his original work focused on the liver (he was attempting to differentiate between tumor types within liver tissue; the work was unsuccessful), he next began to

scan the brain and the benefits of the technique quickly became apparent.

In 1990 another DWI pioneer, Michael Mosely, first reported that the diffusion of water through white matter tracts was anisotropic and he correctly surmised that the best method for describing the directionality of the diffusion would be a tensor(27). The first tractographic studies that could correctly utilize a six-directional approach to tensor calculation (previously, only two directions had been used) were published in 1991(28). Work by Peter Basser and colleagues (funded by the US National Institute of Health) further established the clinical importance of DTI by establishing the capability to demonstrate changes in brain matter composition at the microstructural level(29). Neurons, particularly myelinated ones, have extremely restricted diffusion in a radial direction, while the diffusion is markedly increased in an axial direction. This has allowed diffusion mapping to reconstruct the axonal tracts of the central nervous system in ways not previously possible. Areas of change attributed to cerebrovascular hemmorhage, demyelination, trauma or other abnormal structural alterations will change the DTI signal and has led to several clinical applications. DTI has now proven to be a useful technique in the early detection and localization of stroke and lesions associated with multiple sclerosis (MS)(30). Using DTI in the detection of early changes in AD continues to hold great promise and is a continually evolving field of research.

One of the most significant challenges associated with any type of diffusion-weighted imaging is the high susceptibility of the signal to any type of motion, especially when the subjects (and their MRI signals) are exceptionally small. The location of water molecules (and the fluids they compose) within a living tissue can be influenced by a multitude of factors, not the least of which is the beating of hearts and breathing of air. Early diffusion experiments were fraught with motion artifacts because of so-called, intravoxel-incoherent motions (IVIMs)(31). Because of the complex nature of the signal acquisition sequence, DWI began as an intensely time-consuming process. Techniques for a more rapid acquisition of the diffusion signal were needed to be devised that would reduce this otherwise uncontrollable motion artifact. Echo planar imaging (EPI), devised by Robert Turner and colleagues in the late 1980s, used a unique signal acquisition scheme(32). Traditional MRI acquires data in a “row-by-row” fashion. Data is added sequentially to the k-space (the theoretical 2-D representation of the received radiofrequency signal) by a series of RF pulses; one per row (for example, a 64x64 matrix would be acquired by recieving one signal containing 64 pixels of information (a row) and then repeating this 64 times). EPI uses a single-shot, modulated RF pulse to acquire the entire matrix all at once (imagine a single line that passes through every square of a grid without overlapping or backtracking)(figure 2). This technique has been shown to greatly reduce the effects of IVIM on DWI (and by extension, DTI) scanning and several other, rapid-acquisition techniques (PROPELLER, FLASH, parallel imaging) that also acquire the data much more quickly than conventional MRI(33).

EPI is not without its shortcomings, however. The gradient pulses produced by DTI-EPI MRI can produce eddy currents in the electromagnetic field, particularly as the strength of the magnetic field increases(34). Within a period of two seconds, the large magnetic field has shifted directions over one-hundred times; the process is then repeated using different gradients and different directions in order to construct the tensor. In our experiment, for example, each EPI pulse changed direction 128 times, then was repeated nine times in different orientations to acquire the three A0 images and six B0 images, finally the entire study was repeated 32 times, all using a magnet that is stronger than the Earth's by a

factor of 140 000 (this entire process took 24 minutes). Commonly, many studies using DTI-EPI will utilize a third-party post-processing software that will correct for the distortions and provide a more consistent picture of their data; to be able to discard any “spoiled” images from the dataset before compiling the results is an invaluable step in the post-processing of the data. Of particular use as a post-processing environment is the MATlab program, a robust data analysis and visualization software(35). The program is not for the faint of heart, however, it requires a working knowledge of the computer programming environment and utilizes a programming language (akin to the coding language “Python”) that was not possible to be appropriately learned for this study. As a result, the data was processed using the on-board software included in the Bruker MRI suite. This software did not inherently allow for the same level of detailed data manipulation as a program like MATlab or another commercially-available MRI post-processing suite without again becoming a problem best solved by computer programmers, not clinician-scientists.

Histological analysis of the tissues post-DTI scanning is a critical step in the correlation between the scans acquired and the actual tissues themselves(36). The study intended to section 6μm slices of the left and right hippocampus of each subject animal and prepare them with several types of stain that would be able to localize the pathological deposits associated with AD. The comparison of AD DTI data and the brain tissue histology in human subjects has been a difficult proposition at times. Needless to say, the hippocampus does not lend itself readily to biopsy, nor do all patient's families consent to the autopsies and tissue collection that would be required. Further to this, the time between death of the individual and the collection of tissue also can play an important factor in the viability of tissues, which is why the use of an animal model can provide such an invaluable source of information in studying DTI to detect AD(21). Congo red is a a stain that has shown to bind to amyloid deposits, allowing them to be localized and quantified, while specific monoclonal antibodies that target amyloid precursor protein and tau protein would be able to localize the changes to specific regions of the hippocampus by attaching a fluorescent label to the antibody and quantifying the results using immunohistofluorescence. Due to time constraints, this important step was not completed during the time allotted and will have to be completed at a later date by other members of the lab.

Several fields of study are trying to devise a method of detecting AD in as non-invasive a fashion as possible. Imaging techniques, biomarker assays and sophisticated cognitive assessment strategies are improving our ability to detect AD reliably at a stage where interventions become feasible. In 2011, a joint task force commissioned by the National Institute for Neurological and Communicative Diseases of Stroke (NINCDS) and the Alzheimer's Disease and Related Disorders Association (ADRDA) put forth new recommendations for the diagnosis of dementia due to Alzheimer's disease, including the current consensus on the diagnosis of mild cognitive impairment (MCI) associated with AD as well as pre-clinical Alzheimer's(37). A clinical diagnosis based on well-established criteria remains the most effective way of identifying AD. It also designated two broad classes of AD-related biomarkers; the Biomarkers of β-amyloid accumulation (β-amyloid 42, amyloid precursors, presenilins, apolipoprotein E and other proteins in the amyloid synthesis/degradation pathways) and the Biomarkers of neuronal degeneration and injury (particularly, the Tau family of proteins). Testing for these markers would utilize positron-emission tomography (PET) scanning, or CSF collection, both being particularly invasive techniques compared to MR and not a requirement for diagnosis. Their usefulness, however, in determining whether a pathophysiological process is occurring in the presence of MCI or dementia can be highly supportive of a clinically made AD diagnosis(38). More recently, a longitudinal study of

patients with Autosomal-Dominant Alzheimer's Disease (any mutation to the genes PSEN1, PSEN2 or APP) has demonstrated that temporal trends in the biomarkers of β-amyloid accumulation could be used to predict the onset of clinical symptoms(36). DTI Alzheimer's researchers have been focusing on developing algorithms based on the changes seen in a variety of regions in the brain in order to support the diagnosis of MCI or AD, but have also faced challenges in correctly determining the presence of the earliest stages of the disease(39). One of the biggest challenges facing researchers in these studies is the lack of overlapping structural, biomarker, cognitive and DTI data for their patient population(37). However, as clinician-scientists begin to incorporate more imaging and biomarker information into their research, the sequence of pathophysiological events that lead ultimately to AD moves closer to the day when it is clearly understood and mapped out, allowing even more opportunities for early treatment and drug discovery.

While this study was unsuccessful in demonstrating a significant change in the hippocampus and median entorhinal cortex, the use of DTI in the diagnosis of AD still holds great potential as a non-invasive way of examining the micro-structural environment of the brain. This ability to examine the areas that have both been implicated in the developing pathology of AD without having to harm the patient will only provide more opportunities for intervention in the treatment of Alzheimer's. The potential for DTI to provide the tools we need to identify the development of AD pathology remains and further exploration into this subject is still needed. Statistical modelling has shown that a diagnostic tool that identified AD in patients with sensitivity and specificity of 90 would decrease the individual lifetime risk of Alzheimer's from the current North American estimate of approximately 16.7% for a 65 year-old individual to 10.5%. If the early and reliable diagnosis of AD provides the means to develop a treatment that slowed progression by 50%, the lifetime risk to that individual becomes 5.7%(40). As our population ages, the prevalence of AD, if unchecked, will only increase. The need for reliable techniques to identify cases that are progressing to AD are an important area of current research and will remain an important subject of the study of neurodegenerative disease.

References:

1)Dudgeon, S. (2010). *Rising tide: The impact of dementia on canadian society.* Toronto, ON: Alzheimer's Society of Canada

2)Thiessen, J. D., Glazner, K. A., Nafez, S., Schellenberg, A. E., Buist, R., Martin, M., & Albensi, B. C. (2010). Histochemical visualization and diffusion MRI at 7 tesla in the TgCRND8 transgenic model of alzheimer's disease. *Brain Structure & Function, 215*(1), 29-36

3)Hardy B (2006) Has the Amyloid Cascade Hypothesis for Alzheimer's Disease been Proved? *Journal of Alzheimer's Research*, 3(1), 71-73

4)Nelson PT, Alafuzoff I, Bigio EH, Bouras C, Braak H, Cairns NJ, Castellani RJ, Crain BJ, Davies P, Del Tredici K, Duyckaerts C, Frosch MP, Haroutunian V, Hof PR, Hulette CM, Hyman BT, Iwatsubo T, Jellinger KA, Jicha GA, Kövari E, Kukull WA, Leverenz JB, Love S, Mackenzie IR, Mann DM, Masliah E, McKee AC, Montine TJ, Morris JC, Schneider JA, Sonnen JA, Thal DR, Trojanowski JQ, Troncoso JC, Wisniewski T, Woltjer RL, Beach TG. (2012) Correlation of Alzheimer disease neuropathologic changes with cognitive status: a review of the literature. *J Neuropathol Exp Neurol*. 2012 May;71(5):362-81

5)Yassa MA, Muftuler LT, Stark CE (2010) Ultrahigh-resolution microstructural diffusion tensor imaging reveals perforant path degradation in aged humans in vivo. *Proc Natl Acad Sci U S A* 107, 12687-12691

6)Petersen RC, Smith G, Waring S, Ivnik R, Tangalos E, Kokmen E (1999) Mild cognitive impairment:

clinical characterization and outcome. *Arch Neurol.* 1999; 56:303–8
7)Jagust W. (2006) Positron emission tomography and magnetic resonance imaging in the diagnosis and prediction of dementia. *Alzheimers Dement.* 2006; 2:36–42
8)Khachaturian ZS. (2011) Revised criteria for diagnosis of Alzheimer's disease: National Institute on Aging-Alzheimer's Association diagnostic guidelines for Alzheimer's disease. *Alzheimers Dement.* 2011 May;7(3):253-6
9)Foltz WD, Jaffray DA.(2012) Principles of magnetic resonance imaging. *Radiat Res.* 2012 Apr;177(4):331-48
10)Mori S, Zhang J. (2006) Principles of diffusion tensor imaging and its applications to basic neuroscience research. *Neuron.* 2006 Sep 7;51(5):527-39
11)Le Bihan, D., Mangin, J. F., Poupon, C., Clark, C. A., Pappata, S., Molko, N., & Chabriat, H. (2001). Diffusion tensor imaging: Concepts and applications. *Journal of Magnetic Resonance Imaging : JMRI, 13*(4), 534-546
12)Bozzao, A., Floris, R., Baviera, M. E., Apruzzese, A., & Simonetti, G. (2001). Diffusion and perfusion MR imaging in cases of alzheimer's disease: Correlations with cortical atrophy and lesion load. *AJNR.American Journal of Neuroradiology, 22*(6), 1030-1036s
13)Stefan Skare, Maj Hedehus, Michael E Moseley, Tie-Qiang Li, (2000) Condition Number as a Measure of Noise Performance of Diffusion Tensor Data Acquisition Schemes with MRI, *Journal of Magnetic Resonance,* Volume 147, Issue 2, December 2000, Pages 340-352
14)Denic A, Macura SI, Mishra P, Gamez JD, Rodriguez M, Pirko I. (2011) MRI in rodent models of brain disorders. *Neurotherapeutics.* 2011 Jan;8(1):3-18
15)Bammer R, Skare S, Newbould R, Liu C, Thijs V, Ropele S, Clayton DB, Krueger G, Moseley ME, Glover GH. (2005) Foundations of advanced magnetic resonance imaging. *NeuroRx.* 2005 Apr;2(2):167-96
16)Muller MJ, Greverus D, Dellani PR, Weibrich C, Wille PR, Scheurich A, Stoeter P, Fellgiebel A (2005) Functional implications of hippocampal volume and diffusivity in mild cognitive impairment. *Neuroimage* 28, 1033-1042
17)Oddo, S., Caccamo, A., Shepherd, J. D., Murphy, M. P., Golde, T. E., Kayed, R., Metherate, R., Mattson, M. P., Akbari, Y., & LaFerla, F. M. (2003). Triple-transgenic model of alzheimer's disease with plaques and tangles: Intracellular abeta and synaptic dysfunction. *Neuron, 39*(3), 409-421
18)Patel MR, Klufas RA, Alberico RA, Edelman RR. (1997)Half-fourier acquisition single-shot turbo spin-echo (HASTE) MR: comparison with fast spin-echo MR in diseases of the brain. *AJNR Am J Neuroradiol.* 1997 Oct;18(9):1635-40
19)Lan LM, Yamashita Y, Tang Y, Sugahara T, Takahashi M, Ohba T, Okamura H. (2000) Normal fetal brain development: MR imaging with a half-Fourier rapid acquisition with relaxation enhancement sequence. *Radiology*. 2000 Apr;215(1):205-10
20)Hori M, Ishigame K, Shiraga N, Kumagai H, Aoki S, Araki T. (2008) Mean diffusivity, fractional anisotropy maps, and three-dimensional white-matter tractography by diffusion tensor imaging. Comparison between single-shot fast spin-echo and single-shot echo-planar sequences at 1.5 Tesla. *Eur Radiol.* 2008 Apr;18(4):830-4
21)Olfert, ED, Cross, BM, MacWilliam A (1993) *CCAC Guide to care and use of experimental animals, Vol 1, 2nd Ed.*
22)Fellgiebel A, Yakushev I. (2011) Diffusion tensor imaging of the hippocampus in MCI and early Alzheimer's disease. *J Alzheimers Dis.* 2011;26 Suppl 3:257-62
23)Mielke MM, Kozauer NA, Chan KC, George M, Toroney J, Zerrate M, Bandeen-Roche K, Wang MC, Vanzijl P, Pekar JJ, Mori S, Lyketsos CG, Albert M. (2009) Regionally-specific diffusion tensor imaging in mild cognitive impairment and Alzheimer's disease. *Neuroimage.* 2009; 46:47–55

24)Kline, Morris (1972). *Mathematical thought from ancient to modern times, Vol. 3*. Oxford University Press. pp. 1122–1127
25)Ricci, Gregorio; Levi-Civita, Tullio (1900). "Méthodes de calcul différentiel absolu et leurs applications". *Mathematische Annalen* (Springer) 54 (1–2): 125–201
26)Torrey, H. C. (1956). "Bloch Equations with Diffusion Terms". *Physical Review* **104** (3): 563
27)Moseley; Cohen, Y; Kucharczyk, J; Mintorovitch, J; Asgari, HS; Wendland, MF; Tsuruda, J; Norman, D (1990). "Diffusion-weighted MR imaging of anisotropic water diffusion in cat central nervous system". *Radiology* **176** (2): 439–45
28)Douek, P; Turner, R, Pekar, J, Patronas, N, Le Bihan, D (1991). MR color mapping of myelin fiber orientation. *Journal of computer assisted tomography* **15** (6): 923–9
29)Basser PJ, Pierpaoli C (1996) Microstructural and physiological features of tissues elucidated by quantitative-diffusion tensor MRI. J Magn Reson B 111, 209-219
30)Li TQ, Wahlund LO. (2011) The search for neuroimaging biomarkers of Alzheimer's disease with advanced MRI techniques. *Acta Radiol.* 2011 Mar 1;52(2):211-22
31)Jones DK. (2010) Precision and accuracy in diffusion tensor magnetic resonance imaging. *Top Magn Reson Imaging.* 2010 Apr;21(2):87-99
32)Turner, R; Le Bihan, D, Maier, J, Vavrek, R, Hedges, LK, Pekar, J (1990). "Echo-planar imaging of intravoxel incoherent motion". *Radiology* **177** (2): 407–14
33)Aksoy M, Skare S, Holdsworth S, Bammer R. (2010) Effects of motion and b-matrix correction for high resolution DTI with short-axis PROPELLER-EPI. *NMR Biomed.* 2010 Aug;23(7):794-802
34)Horsfield MA. (1999) Mapping eddy current induced fields for the correction of diffusion-weighted echo planar images. *Magn Reson Imaging.* 1999 Nov;17(9):1335-45
35)MATLAB version 7.10.0. Natick, Massachusetts: *The Mathworks, Inc.2010*

36)Bateman RJ, Xiong C, Benzinger TL, Fagan AM, Goate A, Fox NC, Marcus DS, Cairns NJ, Xie X, Blazey TM, Holtzman DM, Santacruz A, Buckles V, Oliver A, Moulder K, Aisen PS, Ghetti B, Klunk WE, McDade E, Martins RN, Masters CL, Mayeux R, Ringman JM, Rossor MN, Schofield PR, Sperling RA, Salloway S, Morris JC (2012) the Dominantly Inherited Alzheimer Network. Clinical and Biomarker Changes in Dominantly Inherited Alzheimer's Disease. *N Engl J Med.* 2012 Jul 11. [Epub ahead of print]

37)Jack CR Jr, Albert MS, Knopman DS, McKhann GM, Sperling RA, Carrillo MC, Thies B, Phelps CH. (2011) Introduction to the recommendations from the National Institute on Aging-Alzheimer's Association workgroups on diagnostic guidelines for Alzheimer's disease. *Alzheimers Dement.* 2011 May;7(3):257-62
38)Albert MS, DeKosky ST, Dickson D, Dubois B, Feldman HH, Fox NC, Gamst A, Holtzman DM, Jagust WJ, Petersen RC, Snyder PJ, Carrillo MC, Thies B, Phelps CH. (2011) The diagnosis of mild cognitive impairment due to Alzheimer's disease: recommendations from the National Institute on Aging-Alzheimer's Association workgroups on diagnostic guidelines for Alzheimer's disease. *Alzheimers Dement.* 2011 May;7(3):270-9
39)Mesrob L, Sarazin M, Hahn-Barma V, Cruz de Souza L, Dubois B, Gallinari P, Kinkingehun S. (2012) DTI and structural MRI classification in Alzheimer's Disease. *Advances in molecular imaging*, 2012:2, 12-20

40)Clerx L, Visser PJ, Verhey F, Aalten P. (2012) New MRI markers for Alzheimer's disease: a meta-analysis of diffusion tensor imaging and a comparison with medial temporal lobe measurements. J Alzheimers Dis. 2012;29(2):405-29

Ryan Dale

Table 1 – Summary of FA values (scalar value 0-1) for Selected Regions of Interest

	3xTg	*C57*	*Significant?*
Hippocampus (Left)	0.306±0.105	0.363±0.0988	NS
Hippocampus (Right)	0.34±0.114	0.387±0.102	NS
Hippocampus (Total)	0.323±0.155	0.375±0.142	NS
Hemisphere (at -2.20mm from bregma, Left)	0.346±0.142	0.387±0.138	NS
Hemisphere (at -2.20mm from bregma, Right)	0.376±0.139	0.411±0.143	NS
Whole Slice (at -2.20mm from bregma)	0.36±0.143	0.398±0.142	NS
Median Entorhinal Cortex (Left)	0.372±0.0689	0.403±0.0723	NS
Median Entorhinal Cortex (Right)	0.367±0.0798	0.360±0.0596	NS
Median Entorhinal Cortex (Total)	0.370±0.105	0.382±0.0937	NS
Hemisphere (at -4.20mm from bregma, Left)	0.410±0.122	0.420±0.133	NS
Hemisphere (at -4.20mm from bregma, Right)	0.402±0.105	0.405±0.109	NS
Whole Slice (at -4.20mm from bregma)	0.406±0.116	0.412±0.123	NS

Values are given as mean ± SEM *NS = Not Significant*

Table 2 – Summary of MD Values (x10^5 mm^2/s) for Selected Regions of Interest

	3xTg	*C57*	*Significant?*
Hippocampus (Left)	8.27±0.957	8.87±1.48	NS
Hippocampus (Right)	8.73±1.11	8.73±1.83	NS
Hippocampus (Total)	8.5±1.46	8.8±2.35	NS
Hemisphere (at -2.20mm from bregma, Left)	7.6±1.94	8.33±2.30	NS
Hemisphere (at -2.20mm from bregma, Right)	7.87±2.18	7.8±2.54	NS
Whole Slice (at -2.20mm from bregma)	7.77±1.98	8.03±2.51	NS
Median Entorhinal Cortex (Left)	7.17±1.50	8.1±1.24	NS
Median Entorhinal Cortex (Right)	9.13±1.78	9.83±1.79	NS
Median Entorhinal Cortex (Total)	8.15±2.33	8.97±2.18	NS
Hemisphere (at -4.20mm from bregma, Left)	7.13±1.68	7.63±2.12	NS
Hemisphere (at -4.20mm from bregma, Right)	8.3±2.28	8.63±2.16	NS
Whole Slice (at -4.20mm from bregma)	7.73±1.94	8.27±2.24	NS

Values are given as mean ± SEM *NS = Not Significant*

Ryan Dale

Figure 1 – Normal DWI pulse sequence

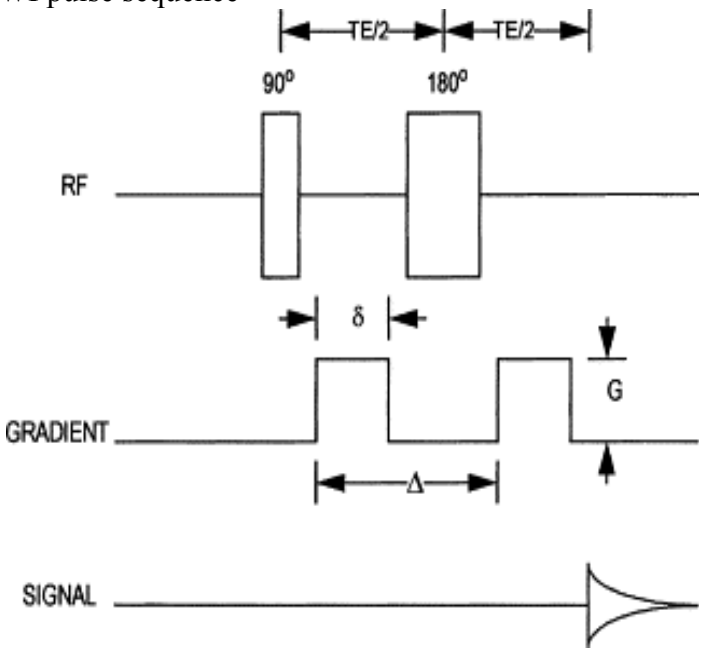

Image credit: Christopher H. Sotak, Nuclear magnetic resonance (NMR) measurement of the apparent diffusion coefficient (ADC) of tissue water and its relationship to cell volume changes in pathological states, Neurochemistry International, Volume 45, Issue 4, September 2004, Pages 569-582

Figure 2 – Normal DTI-EPI single-shot pulse sequence

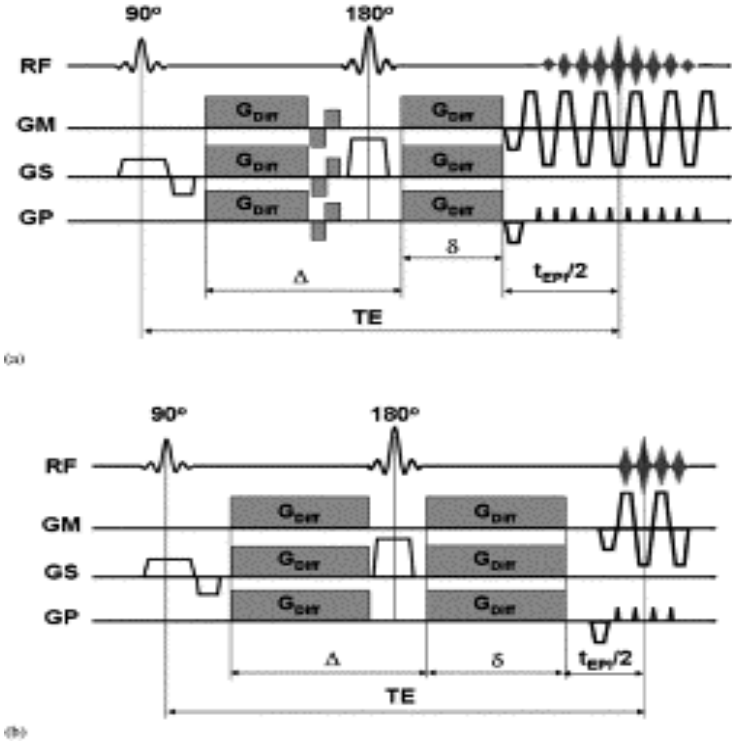

image credit: Roland Bammer, Basic principles of diffusion-weighted imaging, European Journal of Radiology, Volume 45, Issue 3, March 2003, Pages 169-184

Ryan Dale

Figure 3 – A sample RARE scan. The short acquisition time and higher resolution of the scan permits the use of a stereotactic brain atlas to identify that the selected regions of interest will be scanned appropriately by the MRI. Parameters of the image acquisition are listed under Methods and Materials:

Figure 4 – All regions of interest were traced by hand using Bruker software and compared to a stereotactic mouse brain atlas. RARE scans were used to localize the areas of interest, which were then traced to the FA and tensor trace maps.

Figure 4a: ROIs selected at the level of -2.20mm to bregma: Yellow - Right hippocampus; Orange – Left hippocampus; Red – Right hemisphere; Blue – Left hemisphere; Green – Whole slice

Figure 4b: ROIs selected at the level of -4.20mm to bregma: Yellow – Right median entorhinal cortex; Orange – Left median entorhinal cortex; Red – Right hemisphere; Blue – Left hemisphere; Green – Whole slice

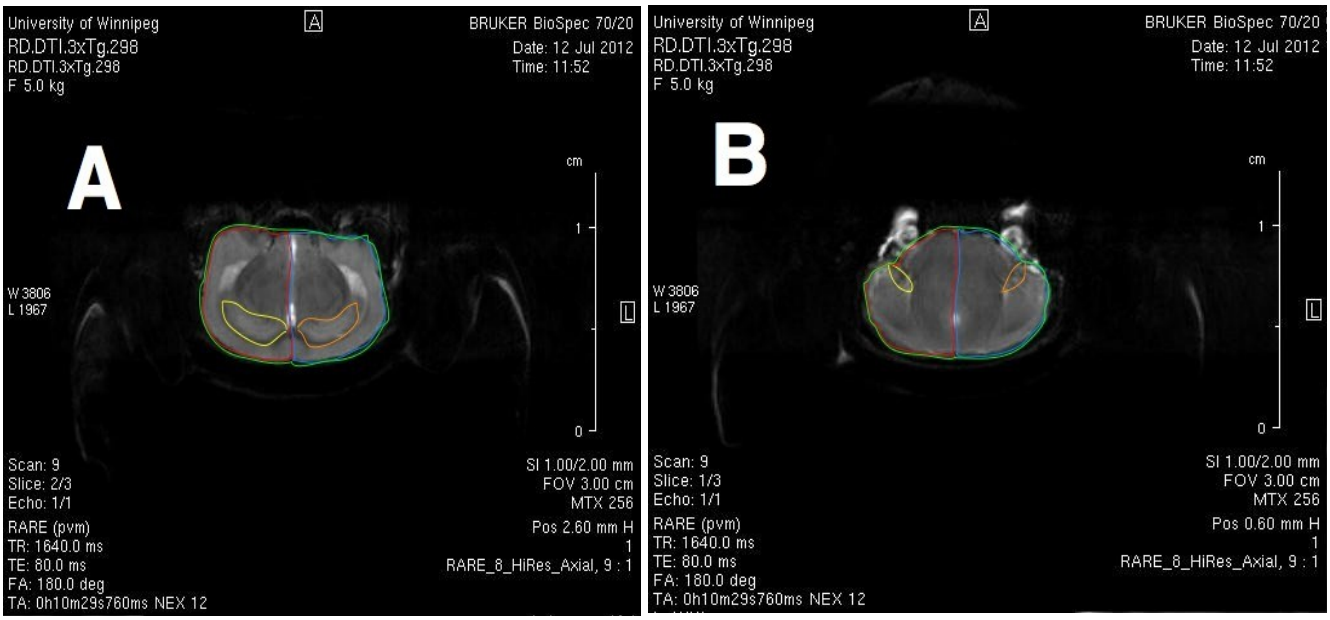

Ryan Dale

Figure 5 – Sample fractional anisotropy maps for DTI-EPI scans. Landmarks on the FA maps are barely present; the use of RARE scans to establish the ROIs were required to correctly differentiate individual regions of each slice.
Figure 5a is FA map at the level of -2.20mm to bregma. *Figure 5b* is the FA map at the level of -4.20mm to bregma. Both images have been cropped at the edges of the cortex to remove areas of noise from the visible field of view.

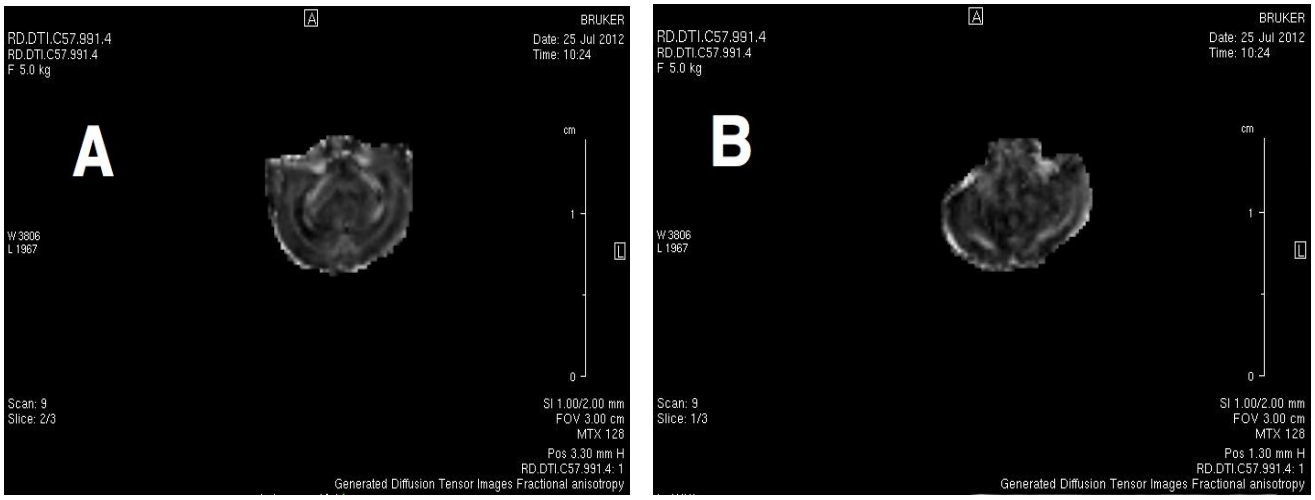

Figure 6 – Sample tensor trace maps for the DTI-EPI scans. Landmarks on the tensor trace maps are entirely indistinguishable; the regions of interest were determined by comparing RARE scan images to a stereotactic brain atlas and then applying parameters for the selected regions to the tensor trace image. The trace is a sum of all three eigenvalues ($\lambda_1 + \lambda_2 + \lambda_3$), the mean diffusivity MD for each scan was calculated by dividing the tensor trace values by 3
Figure 6a is the tensor trace map at the level of -2.20mm to bregma. *Figure 6b* is the tensor trace map at the level of -4.20mm to bregma. Both images have been left un-cropped at the edges of the cortex to demonstrate the level of noise present within the rest of the image within the visible field of view.